Stability Analysis of Interfacial Waves in Hall-Héroult Process: Feasibility Study

Roozbeh Mollaabbasi[1], Donald Ziegler[2], Houshang Alamdari[3], Seyed Mohammad Taghavi[4]

1. Postdoc Researcher
3. Associate Professor
4. Assistant Professor

Aluminum Research Centre REGAL, Laval University, Québec, Canada

2. Program Manager-Modeling

Alcoa Corporation: Aluminum Center of Excellence, Alcoa Technical Center, 859 White Cloud Road, New Kensington, PA 15068

Corresponding author: roozbeh.mollaabbasi.1@ulaval.ca

Abstract

The occurrence of fluid interfacial instabilities due to gravity waves, modified by intense electric/magnetic fields, is one of the important problems in the Hall-Héroult reduction cells. Several parameters affect the flow stability, such as non-uniformity of the walls, density difference, fluid layer thicknesses, wall friction coefficient, magnitude of different forces, etc. In order to analyze the interface stability, first, one can use a two-layer thin-film fluid flow model inside a simplified uniform 2D geometry, while considering the effects of electro-magnetic fields as a source term in the momentum equation. In this study, we explore the possibility of a stability analysis of interfacial waves in Hall-Héroult process by applying a weighted residual model to find the marginal stability of the system at the long-wave length limit. Finally, we numerically analyze the effects of non-uniform lower walls on the convective instability of the interface. The results show that the proposed model can be used to predict the effects of different geometrical parameters as well as operational ones on the stability of cryolite-aluminum interface in the Hall-Héroult process.

Keywords: Hall-Héroult reduction cells, stability analysis, two-phase flow, two-layer model.

1. Introduction

Hall-Héroult process is one of the major industrial process for smelting aluminum. This process is very complex due the presence of hydro-, electro-, magnetohydro-dynamic features, as well as electro-chemical effects. One important problem is the occurrence of fluid interfacial instabilities within the Hall-Héroult reduction cells, due to gravity waves modified by intense electric/magnetic fields. There are many parameters that can affect the stability of the flow, e.g., magnitude of various forces, density difference, fluid layer thicknesses, wall friction coefficient, etc. We simplify the magnetic field and the current that passes through the layers in order to simplify the problem and examine the feasibility of stability analysis of interfacial waves in Hall-Héroult process.

Two-layer, shallow fluid flow inside a simplified 2D geometry with two Newtonian fluids (Aluminum and Cryolite) can be considered as a powerful tool to capture the interfacial instability [1]. Here, two fluids can be assumed immiscible, with a small density difference. The momentum and continuity equations can be developed for both fluids.

Bojarevics has developed a model considering a variable cathode height, where the effects of fluid height on the horizontal current density and wave development was studied [3]. Compared to the previous works on the Hall-Héroult process modeling flows [4, 5, 6, 7], the contribution of this work will be to develop a novel, semi-analytical model to deliver the condition of the

instability of the system while taking into account magnetic effects with non-uniform boundary conditions. In particular, non-uniform boundary conditions at the bottom of the flow geometry (cathode block surface) will be considered. A weighted residual model (WRM) [2] approach will be applied to the system to consider weak inertial effects on the flow stability [1]. The results will deliver in particular the threshold for the operating conditions for the Hall-Héroult process, in which fluid interfacial instabilities are avoided. The model will also provide an understanding how the interfacial perturbation may grow, versus the dimensionless groups that govern the flow.

2. Modeling

Figure 1 illustrates a simple schematic of the aluminum production cell. In this system, several parameters affect the instability of the interface between the aluminium and cryolite layers such as the magnetic field and the current that passes through the layers, the non-uniform geometry, two different fluids with different density, etc.

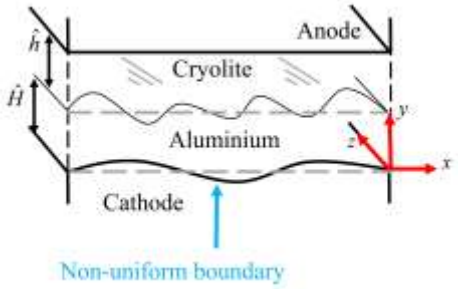

Figure 1. Schematic of an aluminium production cell.

Assuming the electro-magnetic force is dominant in the aluminium layer, we simplify the problem to a system of two layers of fluids in a non-uniform geometry.

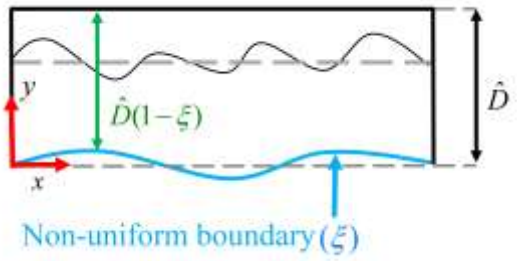

Figure 2. Flow configuration in a non-uniform geometry.

Figure 2 shows schematically the flow configuration in the vertical (*x, y*) plane. Here, the upper wall is uniform and the lower wall is considered non-uniform. The local height of the cell varies in *x* direction as $\hat{D}(1-\xi)$, in which $\hat{D}$ is the height of the imaginary uniform geometry and ξ is the non-uniformity function of the lower wall. We consider two Newtonian fluids with different densities ($\hat{\rho}_1, \hat{\rho}_2$) and viscosities ($\hat{\mu}_1, \hat{\mu}_2$). Layers 1 and 2 are taken to correspond to the lower and upper layer, respectively.

We can write the momentum and continuity equations for each layer in the *x* and *y* direction as:

$$\hat{\rho}_1\left(\frac{\partial \hat{u}_1}{\partial \hat{t}} + \hat{u}_1\frac{\partial \hat{u}_1}{\partial \hat{x}} + \hat{v}_1\frac{\partial \hat{u}_1}{\partial \hat{y}}\right) = -\frac{\partial \hat{p}_1}{\partial \hat{x}} + \hat{\mu}_1\left[\frac{\partial \hat{u}_1^{\,2}}{\partial \hat{x}^2} + \frac{\partial \hat{u}_1^{\,2}}{\partial \hat{y}^2}\right] + \hat{F}, \tag{1}$$

$$\hat{\rho}_2\left(\frac{\partial \hat{u}_2}{\partial \hat{t}} + \hat{u}_2\frac{\partial \hat{u}_2}{\partial \hat{x}} + \hat{v}_2\frac{\partial \hat{u}_2}{\partial \hat{y}}\right) = -\frac{\partial \hat{p}_2}{\partial \hat{x}} + \hat{\mu}_2\left[\frac{\partial \hat{u}_2^{\,2}}{\partial \hat{x}^2} + \frac{\partial \hat{u}_2^{\,2}}{\partial \hat{y}^2}\right], \tag{2}$$

$$\hat{\rho}_1\left(\frac{\partial \hat{v}_1}{\partial \hat{t}}+\hat{u}_1\frac{\partial \hat{v}_1}{\partial \hat{x}}+\hat{v}_1\frac{\partial \hat{v}_1}{\partial \hat{y}}\right)=-\frac{\partial \hat{p}_1}{\partial \hat{y}}+\hat{\mu}_1\left[\frac{\partial \hat{v}_1^{\,2}}{\partial \hat{x}^2}+\frac{\partial \hat{v}_1^{\,2}}{\partial \hat{y}^2}\right]-\hat{\rho}_1\hat{g}, \tag{3}$$

$$\hat{\rho}_2\left(\frac{\partial \hat{v}_2}{\partial \hat{t}}+\hat{u}_2\frac{\partial \hat{v}_2}{\partial \hat{x}}+\hat{v}_2\frac{\partial \hat{v}_2}{\partial \hat{y}}\right)=-\frac{\partial \hat{p}_2}{\partial \hat{y}}+\hat{\mu}_2\left[\frac{\partial \hat{v}_2^{\,2}}{\partial \hat{x}^2}+\frac{\partial \hat{v}_2^{\,2}}{\partial \hat{y}^2}\right]-\hat{\rho}_2\hat{g}, \tag{4}$$

$$\frac{\partial \hat{u}_1}{\partial \hat{x}}+\frac{\partial \hat{v}_1}{\partial \hat{y}}=0, \tag{5}$$

$$\frac{\partial \hat{u}_2}{\partial \hat{x}}+\frac{\partial \hat{v}_2}{\partial \hat{y}}=0, \tag{6}$$

where, $\hat{u},\hat{v},\hat{p},\hat{g}$ and $\hat{F}$ are the velocity component in the *x* direction, the velocity component in the *y* direction, the pressure, the gravitational acceleration and a body force that is the proportion of the gradient of electro-magnetic force. We consider the following dimensionless parameters

$$x=\frac{\hat{x}}{\hat{D}(1-\xi)},\ y=\frac{\hat{y}}{\hat{D}(1-\xi)},\ u=\frac{\hat{u}}{\frac{\hat{u}_0}{(1-\xi)}},\ v=\frac{\hat{v}}{\frac{\hat{u}_0}{(1-\xi)}},\ t=\frac{\hat{t}}{\hat{D}(1-\xi)/\frac{\hat{u}_0}{(1-\xi)}},\ p=\frac{\hat{p}}{\frac{\frac{\hat{u}_0}{(1-\xi)}\hat{\mu}_1}{\hat{D}(1-\xi)}}, \tag{7}$$

where, $\hat{u}_0$ is the average velocity in the imaginary uniform geometry. We make the momentum equations dimensionless as:

$$\mathrm{Re}(1+\mathrm{At})\left(\frac{\partial u_1}{\partial t}+u_1\frac{\partial u_1}{\partial x}+v_1\frac{\partial u_1}{\partial y}\right)=-\frac{\partial p_1}{\partial x}+\left[\frac{\partial u_1^{\,2}}{\partial x^2}+\frac{\partial u_1^{\,2}}{\partial y^2}\right]+\chi, \tag{8}$$

$$\mathrm{Re}(1-\mathrm{At})\left(\frac{\partial u_2}{\partial t}+u_2\frac{\partial u_2}{\partial x}+v_2\frac{\partial u_2}{\partial y}\right)=-\frac{\partial p_2}{\partial x}+m\left[\frac{\partial u_2^{\,2}}{\partial x^2}+\frac{\partial u_2^{\,2}}{\partial y^2}\right], \tag{9}$$

$$\mathrm{Re}(1+\mathrm{At})\left(\frac{\partial v_1}{\partial t}+u_1\frac{\partial v_1}{\partial x}+v_1\frac{\partial v_1}{\partial y}\right)=-\frac{\partial p_1}{\partial y}+\left[\frac{\partial v_1^{\,2}}{\partial x^2}+\frac{\partial v_1^{\,2}}{\partial y^2}\right]-\frac{\mathrm{Re}}{Fr^2}, \tag{10}$$

$$\mathrm{Re}(1-\mathrm{At})\left(\frac{\partial v_2}{\partial t}+u_2\frac{\partial v_2}{\partial x}+v_2\frac{\partial v_2}{\partial y}\right)=-\frac{\partial p_2}{\partial y}+m\left[\frac{\partial v_2^{\,2}}{\partial x^2}+\frac{\partial v_2^{\,2}}{\partial y^2}\right]+\frac{\mathrm{Re}}{Fr^2}, \tag{11}$$

$$\frac{\partial u_1}{\partial X}+\frac{\partial v_1}{\partial y}=0, \tag{12}$$

$$\frac{\partial u_2}{\partial X}+\frac{\partial v_2}{\partial y}=0, \tag{13}$$

where,

$$\mathrm{Re}=\frac{\hat{u}_0\hat{D}(\hat{\rho}_1+\hat{\rho}_2)}{2\hat{\mu}_1}=\mathrm{Re}^*,\ Fr=\frac{\hat{u}_0/(1-\xi)}{\sqrt{At\,\hat{g}\hat{D}(1-\xi)}}=Fr^*(1-\xi)^{-3/2},\ At=\frac{\hat{\rho}_1-\hat{\rho}_2}{\hat{\rho}_1+\hat{\rho}_2},\ m=\frac{\hat{\mu}_2}{\hat{\mu}_1},$$

$$\chi=\frac{\hat{D}^2(1-\xi)^3}{\hat{u}_0\hat{\mu}_1}\hat{F}=\chi^*(1-\xi)^3$$

and * denotes the corresponding value in a uniform channel geometry. We assume that the interface elongation is over a dimensionless length scale ($\delta = \frac{Fr^2}{\mathrm{Re}}$) in order to scale our equations [8] where $\hat{L}$ is the characteristic spreading length.

We rescale the governing equations following the standard methods using $\delta x = X, \delta t = T$, $\delta p = P, v = \delta V$ to derive a perturbation approximation.

$$\delta \,\mathrm{Re}(1+\mathrm{At})(\frac{\partial u_1}{\partial T} + u_1 \frac{\partial u_1}{\partial X} + V_1 \frac{\partial u_1}{\partial y}) = -\frac{\partial P_1}{\partial X} + \frac{\partial u_1^{\,2}}{\partial y^2} + \chi + O(\delta^2), \tag{14}$$

$$\delta \,\mathrm{Re}(1-\mathrm{At})(\frac{\partial u_2}{\partial T} + u_2 \frac{\partial u_2}{\partial X} + V_2 \frac{\partial u_2}{\partial y}) = -\frac{\partial P_2}{\partial X} + m\frac{\partial u_2^{\,2}}{\partial y^2} + O(\delta^2), \tag{15}$$

$$\delta^3 \,\mathrm{Re}(1+\mathrm{At})(\frac{\partial V_1}{\partial T} + u_1 \frac{\partial V_1}{\partial X} + V_1 \frac{\partial V_1}{\partial y}) = -\frac{\partial P_1}{\partial y} - 1 + O(\delta^4) + O(\delta^2), \tag{16}$$

$$\delta^3 \,\mathrm{Re}(1-\mathrm{At})(\frac{\partial V_2}{\partial T} + u_2 \frac{\partial V_2}{\partial X} + V_2 \frac{\partial V_2}{\partial y}) = -\frac{\partial P_2}{\partial y} + 1 + O(\delta^4) + O(\delta^2). \tag{17}$$

Considering $\delta \to 0$ while keeping $\delta\,\mathrm{Re}$ and putting m = 1, the momentum equations could be simplified as:

$$\delta \,\mathrm{Re}(1+\mathrm{At})(\frac{\partial u_1}{\partial T} + u_1 \frac{\partial u_1}{\partial X} + V_1 \frac{\partial u_1}{\partial y}) = -\frac{\partial P_1}{\partial X} + \frac{\partial u_1^{\,2}}{\partial y^2} + \chi, \tag{18}$$

$$\delta \,\mathrm{Re}(1-\mathrm{At})(\frac{\partial u_2}{\partial T} + u_2 \frac{\partial u_2}{\partial X} + V_2 \frac{\partial u_2}{\partial y}) = -\frac{\partial P_2}{\partial X} + m\frac{\partial u_2^{\,2}}{\partial y^2}, \tag{19}$$

$$0 = -\frac{\partial P_1}{\partial y} - 1, \tag{20}$$

$$0 = -\frac{\partial P_2}{\partial y} + 1, \tag{21}$$

$$\frac{\partial u}{\partial X} + \frac{\partial V}{\partial y} = 0. \tag{22}$$

where, $P_0(\mathrm{X},\mathrm{T}) = \mathrm{P}(\mathrm{X},0,\mathrm{T}) - \mathrm{X}\,\chi$. The conservation of mass in the system will be written as:

$$\int_0^h u_1 dy + \int_h^1 u_2 dy = 1. \tag{23}$$

The interface height (h) evolution is captured by the kinematic condition equation as:

$$\frac{\partial h}{\partial T} + \frac{\partial q}{\partial X} = 0, \tag{24}$$

where, q is the flux function.

We can define the velocity profile of each layer as a function of the aspect ratio [8] as:

$$u_i(X, y, T) = u_i^{(0)} + \delta u_i^{(1)} + O(\delta^2), \quad i = 1, 2. \tag{25}$$

Substituting this expansion into the momentum equations (Equation (14) and Equation (15)) and assuming that the leading-order solutions, $u_i^{(0)}$ are maximum of degree two in y, we find

$$u_i^{(0)} = A_i(X,T)y^2 + B_i(X,T)y + C_i(X,T), \quad i = 1,2, \tag{26}$$

with the mentioned coefficients [7], the momentum equations can be integrated by having fixed the dependence of the leading order streamwise velocity components on y. The analysis becomes easier by multiplication of the momentum equations in some suitable weight functions, $g_i(X,y,T)$ such that unknown higher order terms are eliminated. Therefore, we have to define the weight functions in the way that the averaged equations are no longer dependent on the first-order terms in the velocity field expansion (Equation 25) [9]. The sufficient conditions of the weight functions are [10]:

$$\begin{gathered} \int_0^h g_1 dy + \int_h^1 g_2 dy = 0, \frac{\partial g_1}{\partial y}\Big|_{y=h} - \frac{\partial g_2}{\partial y}\Big|_{y=h} = 0, \\ g_1(X,h,T) = g_2(X,h,T), g_1(X,0,T) = g_2(X,1,T) = 0, \end{gathered} \tag{27}$$

We consider g_i as a polynomial in y (assuming the second order of magnitude):

$$g_i(X,y,T) = D_i(X,T)y^2 + E_i(X,T)y + F_i(X,T), \quad i = 1,2. \tag{28}$$

Using double integration by parts on the momentum equations and summing them results,

$$\begin{aligned} &\int_0^h \left[\delta(1+\mathrm{At})\mathrm{Re}\left(\frac{\partial u_1^{(0)}}{\partial T} + u_1^{(0)}\frac{\partial u_1^{(0)}}{\partial X} + V_1^{(0)}\frac{\partial u_1^{(0)}}{\partial y}\right) - \frac{\partial^2 u_1^{(0)}}{\partial y^2} - \chi \right] g_1 dy \\ &+ \int_h^1 \left[\delta(1-\mathrm{At})\mathrm{Re}\left(\frac{\partial u_2^{(0)}}{\partial T} + u_2^{(0)}\frac{\partial u_2^{(0)}}{\partial X} + V_2^{(0)}\frac{\partial u_2^{(0)}}{\partial y}\right) - \frac{\partial^2 u_2^{(0)}}{\partial y^2} - \frac{\partial h}{\partial X} \right] g_2 dy = 0. \end{aligned} \tag{29}$$

Substituting Equation (26) and the weighted functions with respect to their coefficients into Equation (28) along with the use of kinematic condition results in the following system of equations:

$$\begin{gathered} \frac{\partial h}{\partial T} + \frac{\partial q}{\partial X} = 0, \\ R_1\frac{\partial h}{\partial T} + R_2\frac{\partial h}{\partial X} + R_3\frac{\partial q}{\partial T} + R_4\frac{\partial q}{\partial X} + R_5 = 0. \end{gathered} \tag{30}$$

Here, R_1, R_2, R_3, R_4 and R_5 are the coefficients of Equation (30) which are functions of q and h (see Taghavi et al. [1] for these functions and more details).

Now, we can analyze the growth of instabilities at the interface. To do so, we use Equation (30) and solve an initial value problem. We fix the initial value (h_s) as the steady state interface height. Then we perturb the initial condition with a wave (we take the amplitude of 0.05). Now, we track the response of the system to this perturbation to see if the interface amplitude grows or decays in time and space [11].

3. Results and discussion

In this part, first, we compare the results of the developed model with the literature in order to validate our model. Figure 3 gives a comparison between the analytical approach (the blue line) [1] and the numerical approach from our model in a uniform geometry. It shows the stability diagram indicating stable flows (black triangle) and unstable flows (red square) in a uniform geometry. The blue line indicates the neutral curve for the long-wavelength limit for the interface initially located at $h_s = 0.2$ (a), $h_s = 0.5$ (b) and $h_s = 0.6$ (c). This comparison indicates, there is a good agreement between the results of marginal stability (the blue line) and convective instability analysis.

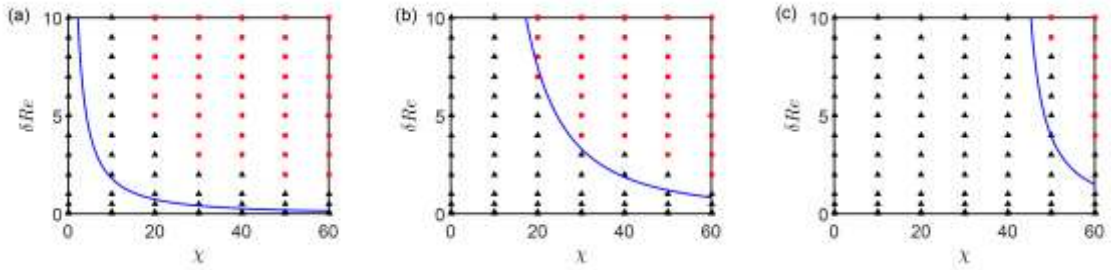

Figure 3. Stability diagram indicating stable flows (black triangle) and unstable flows (red square) in a uniform geometry. The line indicates the neutral curve for the long-wavelength limit for the interface initially located at h_s = 0.2 (a), h_s = 0.5 (b) and h_s = 0.6.

After the validation of the model, we have chosen four different non-uniform geometries (two wavy wall with different wave numbers, one arbitrary wall and one lego wall [12]) in order to study the effects of non-uniform lower wall on the stability of the interface. Here, there is not any analytical solution for marginal instability and we should rely on the numerical approach.

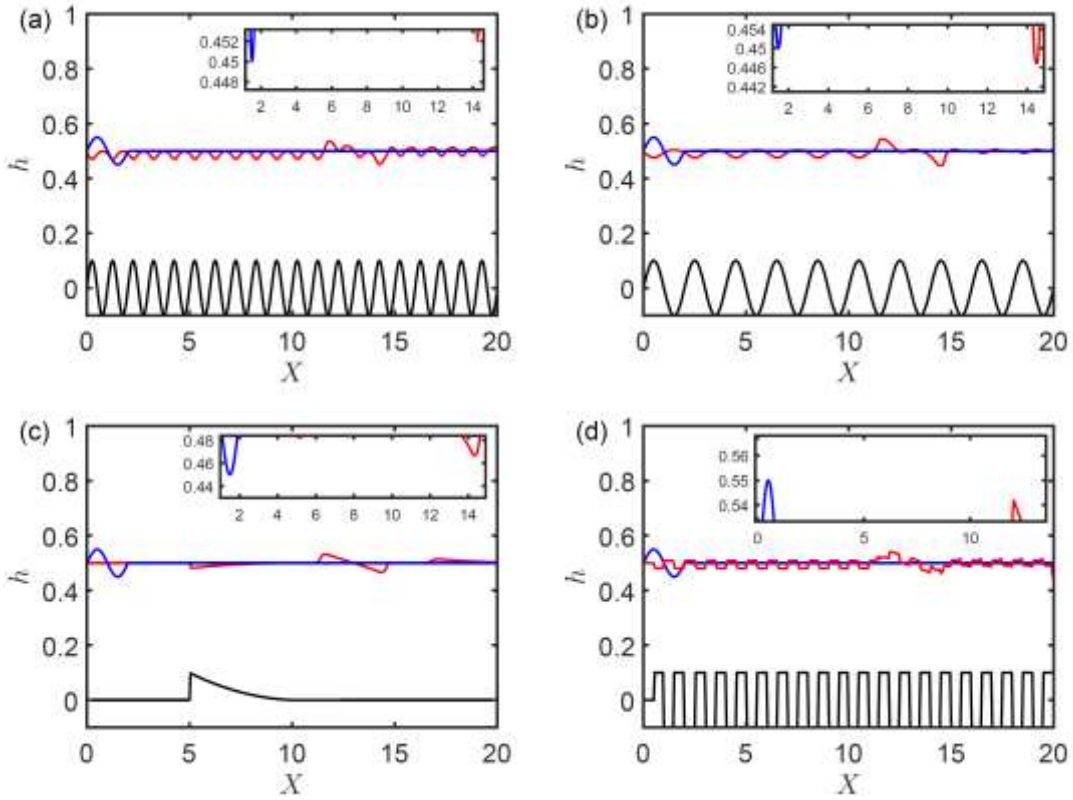

Figure 4. Effects of the lower wall on convective instability of the interface. The lower wall changes with different arbitrary equations. (a) $y = 0.1\sin(2\pi X)$, (b) $y = 0.1\sin(\pi X)$, (c) $y = 0.0034X^2 - 0.0709X + 0.3692$ for $5 \le X \le 10$ and (d) step function. The blue line shows the initial perturbation applied to the system and the red line is the perturbed interface after T = 8. h_s =0.5, χ^* = 35 and δRe = 1 in all cases.

We have applied the initial perturbation on the governing equations and tracked in time to study the convective instability of those non-uniform geometries. Figure (4) shows the effect of the lower wall on convective instability of the interface. The lower wall changes with different arbitrary equations such as: $y = 0.1\sin(2\pi X)$, (b) $y = 0.1\sin(1\pi X)$, (c) $y = 0.0034X^2 - 0.0709X + 0.3692$ for $5 \le X \le 10$ and (d) step function [12]. The blue line shows the initial perturbation as applied to the system and the red line is the perturbed interface after $T = 8$. $h_s = 0.5$, $\chi^* = 35$ and

δRe = 1 in all cases. Comparing Figure 4a and Figure 3 shows that the interface is still stable while decreasing the wave number of the lower wall destabilizes the interface (see Figure 4b). In addition, the arbitrary wall (Figure 4c) and the logo shape wall damp the initial perturbation along the time. To study the effect of the non-uniform lower wall on the instability of the interface, we can complete the diagram of δRe versus χ^*.

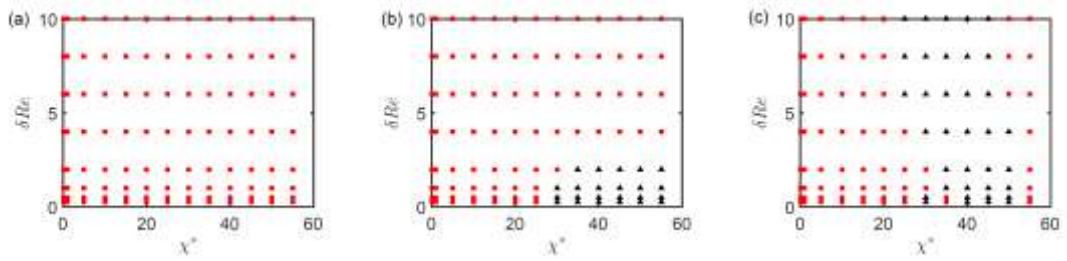

Figure 5. Stability diagram indicating stable flows (black triangle) and unstable flows (red square) in a non-uniform geometry (y = 0.1sin (2πX) is used to produce non-uniformity in the lower wall) at different h_s (h_s = 0.2 (a), h_s = 0.5 (b) and h_s = 0.6 (c)).

Here, we compare the stability analysis results of wavy wall geometries at two different wave numbers. Figure 5 shows the stability diagram indicating stable flows (black triangle) and unstable flows (red square) in a non-uniform geometry at different h_s when the lower wall is y = 0.1sin (2πX). Comparing these results with Figure 3 points out that the configuration of the stable and unstable zones are completely different in uniform and non-uniform geometries. Figure 6 shows that the stable zone shrinks for all three h_s values and the interface becomes more unstable by decreasing the wave number of the lower wall (y = 0.1sin (1πX)).

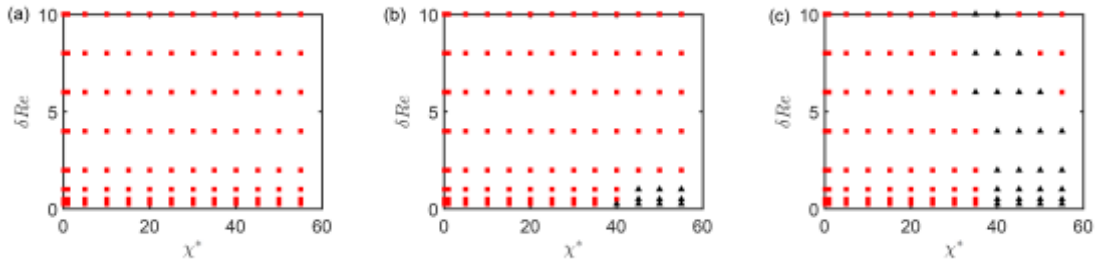

Figure 6. Stability diagram indicating stable flows (black triangle) and unstable flows (red square) in a non-uniform geometry (y = 0.1sin (1πX) is used to produce non-uniformity in the lower wall) at h_s = 0.2 (a), h_s = 0.5 (b) and h_s = 0.6 (c).

4. Conclusion

A semi-analytical approach to analyze the convective stability in a Hall-Héroult reduction cell is a powerful tool in capturing the instability of the interface. The non-uniformity of the lower wall dramatically affects the stability of the interface. Comparing the results of a uniform geometry with a non-uniform geometry (wavy lower wall) shows the stable zone shrinks and the interface becomes more unstable by decreasing the wave number of the lower wall.

5. Acknowledgment

This research has been carried out at Université Laval, supported financially by an NSERC Engage grant. The authors acknowledge Alcoa for the support of this work.

6. References

1. Seyed M. Taghavi et al., Miscible displacement flows in near-horizontal ducts at low Atwood number, *Journal of Fluid Mechanics,* Vol. 696 (2012), 175-214.
2. Kamran Alba, Seyed M. Taghavi and Ian A. Frigaard, A weighted residual method for two-layer non-Newtonian channel flows: steady-state results and their, *Journal of Fluid Mechanics,* Vol. 731 (2013), 509-544.
3. Valdis Bojarevics and Kulis Pericleous, Shallow water model for aluminium electrolysis cells with variable top and bottom, *Light Metals* 2008, 403-408.
4. Thorleif Sele, Instabilities of the Metal Surface in Electrolytic Alumina Reduction Cells, *Light Metals* 1997, 613-618.
5. Nobuo Urata, Magnetics and metal pad instability, *Essential Readings in Light Metals*, 2016, 330-335.
6. Alfred D. Sneyd and A. Wang, Interfacial instability due to MHD mode coupling in aluminium reduction cells, *Journal of Fluid Mechanics,* Vol. 263 (1994), 343-360.
7. Peter A. Davidson and R. I. Lindsay, Stability of interfacial waves in aluminium reduction cells, *Journal of Fluid Mechanics,* Vol. 362 (1998), 273-295.
8. Roozbeh Mollaabbasi and Seyed M. Taghavi., Buoyant displacement flows in slightly non-uniform channels, *Journal of Fluid Mechanics,* Vol. 795 (2016), 876-913.
9. Kamran Alba, Patrice Laure and Roger E. Khayat, Transient two-layer thin-film flow inside a channel, *Physical Review E,* Vol. 84 (2011), 026320-1-14.
10. Mustapha Amaouche, Nadia Mehidi and Nawel Amatousse, Linear stability of a two-layer film flow down an inclined channel: A second-order weighted residual approach, *Physics of Fluids,* Vol. 8 (2007), 084106.
11. Philip Drazin and W.H. Reid, Hydrodynamic stability, *Cambridge University Press* 2004.
12. Andrey Yurkov, Refractories and carbon cathode materials for aluminium reduction cells, *Refractories for aluminium,* 2015, 65-208.